

# Squeezed correlations of $\phi$ meson pairs for hydrodynamic sources in high-energy heavy-ion collisions

Yong Zhang<sup>1</sup>, Jing Yang<sup>1</sup>, and Wei-Ning Zhang<sup>1,2,\*</sup>

<sup>1</sup>*School of Physics and Optoelectronic Technology,  
Dalian University of Technology, Dalian, Liaoning 116024, China*

<sup>2</sup>*Department of Physics, Harbin Institute of Technology,  
Harbin, Heilongjiang 150006, China*

## Abstract

In the hot and dense hadronic sources formed in high-energy heavy-ion collisions, the particle interactions in medium might lead to a squeezed back-to-back correlation (BBC) of boson-antiboson pairs. We calculate the BBC functions of  $\phi\phi$  for sources evolving hydrodynamically in  $(2 + 1)$  dimensions and with longitudinal boost invariance. The BBC functions for hydrodynamic sources exhibit oscillations as a function of the particle momentum because the temporal distributions of hydrodynamic sources have sharp falls to 0 at large evolving times. The dependences of the BBC functions on the directions of the particle momentum are investigated. For transverse anisotropic sources, the BBC functions are minimum when the azimuthal angles of the particles reach 0. The BBC functions increase with decreasing absolute value of the particle pseudorapidity. The oscillations and the dependences on the particle azimuthal angle and pseudorapidity are the significant signatures for detecting the BBC in high-energy heavy-ion collisions.

PACS numbers: 25.75.Gz, 25.75.Ld, 21.65.jk

---

\* wnzhang@dlut.edu.cn

## I. INTRODUCTION

In the hot and dense hadronic sources formed in high energy heavy ion collisions, the mass modification of particles in medium can lead to a squeezed back-to-back correlation (BBC) of the boson-antiboson pair [1, 2]. This BBC is the result of a quantum mechanical transformation relating in-medium quasiparticles to the two-mode squeezed states of their free observable counterparts, through a Bogoliubov transformation between the creation (annihilation) operators of the quasiparticles and the free observable particles [1–3]. The investigations of the BBC of boson-antiboson pairs may provide a new way for people to understand the thermal and dynamical properties of the hadronic sources in high energy heavy ion collisions.

Denote  $a_{\mathbf{k}}$  ( $a_{\mathbf{k}}^\dagger$ ) the annihilation (creation) operator of the free boson with momentum  $\mathbf{k}$  and mass  $m$ , and  $b_{\mathbf{k}}$  ( $b_{\mathbf{k}}^\dagger$ ) the annihilation (creation) operator of the corresponding quasiparticle with momentum  $\mathbf{k}$  and modified mass  $m_*$  in homogeneous medium; they are related by the Bogoliubov transformation [1, 2]

$$a_{\mathbf{k}} = c_{\mathbf{k}} b_{\mathbf{k}} + s_{-\mathbf{k}}^* b_{-\mathbf{k}}^\dagger, \quad (1)$$

where

$$c_{\mathbf{k}} = \cosh f_{\mathbf{k}}, \quad s_{\mathbf{k}} = \sinh f_{\mathbf{k}}, \quad f_{\mathbf{k}} = \frac{1}{2} \log(\omega_{\mathbf{k}}/\Omega_{\mathbf{k}}), \quad (2)$$

$$\omega_{\mathbf{k}} = \sqrt{\mathbf{k}^2 + m^2}, \quad \Omega_{\mathbf{k}} = \sqrt{\mathbf{k}^2 + m_*^2}. \quad (3)$$

The BBC function is defined as [1, 2]

$$C(\mathbf{k}, -\mathbf{k}) = 1 + \frac{|G_s(\mathbf{k}, -\mathbf{k})|^2}{G_c(\mathbf{k}, \mathbf{k})G_c(-\mathbf{k}, -\mathbf{k})}, \quad (4)$$

where  $G_c(\mathbf{k}_1, \mathbf{k}_2)$  and  $G_s(\mathbf{k}_1, \mathbf{k}_2)$  are the chaotic and squeezed amplitudes, respectively,

$$G_c(\mathbf{k}_1, \mathbf{k}_2) = \sqrt{\omega_{\mathbf{k}_1}\omega_{\mathbf{k}_2}} \langle a_{\mathbf{k}_1}^\dagger a_{\mathbf{k}_2} \rangle, \quad (5)$$

$$G_s(\mathbf{k}_1, \mathbf{k}_2) = \sqrt{\omega_{\mathbf{k}_1}\omega_{\mathbf{k}_2}} \langle a_{\mathbf{k}_1} a_{\mathbf{k}_2} \rangle, \quad (6)$$

where  $\langle \dots \rangle$  indicates the ensemble average. The BBC function for a homogeneous source with volume  $V$  and temperature  $T$  can be expressed as [2]

$$C(\mathbf{k}, -\mathbf{k}) = 1 + \frac{V |c_{\mathbf{k}} s_{\mathbf{k}}^* n_{\mathbf{k}} + c_{-\mathbf{k}} s_{-\mathbf{k}}^* (n_{-\mathbf{k}} + 1)|^2}{V [n_1(\mathbf{k}) n_1(-\mathbf{k})]}, \quad (7)$$

where

$$n_{\mathbf{k}} = \frac{1}{\exp(\Omega_{\mathbf{k}}/T) - 1}, \quad (8)$$

$$n_1(\mathbf{k}) = |c_{\mathbf{k}}|^2 n_{\mathbf{k}} + |s_{-\mathbf{k}}|^2 (n_{-\mathbf{k}} + 1). \quad (9)$$

In Ref. [3], S. Padula *et al.* put forward the formulism of the BBC function for the local-equilibrium evolving system and studied the BBC functions of  $\phi\phi$  for expanding sources with a Gaussian space profile. Recently, the BBC functions of  $K^+K^-$  were investigated [4] for expanding Gaussian sources, and a method was suggested [5] to search for the squeezed BBC in heavy-ion collisions at the Relativistic Heavy Ion Collider (RHIC) and the Large Hadron Collider (LHC). In Refs. [6] and [7], we calculated the BBC functions of relativistic  $\phi\phi$  and  $K^+K^-$  pairs for spherical and ellipsoid expanding Gaussian sources. The relativistic effect on the BBC functions [6] and the dependence of the BBC functions on the direction of the particle momentum for the anisotropic sources [7] are investigated. However, all the source density distributions used in the calculations in previous works are space-time separated, having Gaussian spatial distributions and an independent temporal distribution of exponential decay or others [3–7]. Investigations of the BBC based on more realistic space-time evolving source models will be of interest in high-energy heavy-ion collisions.

Relativistic hydrodynamics has been extensively applied to high-energy heavy-ion collisions. In this work, we use the ideal relativistic hydrodynamics in  $2 + 1$  dimensions to describe the transverse expansion of sources with zero net baryon density and combine the Bjorken boost-invariant hypothesis [8] for the source longitudinal evolution. As a first step to the study of the BBC for a more realistic source model, these descriptions are suitable for the heavy-ion collisions at the RHIC top energy and the LHC energy [9–21]. We investigate the BBC functions of  $\phi$  meson pairs for the hydrodynamic sources. The results indicate that the BBC functions of  $\phi\phi$  exhibit oscillations as a function of the particle momentum and vary with the particle azimuthal angle and pseudorapidity. The oscillations and the dependences on particle azimuthal angle and pseudorapidity are the significant signatures for detecting the BBC in high-energy heavy-ion collisions.

The rest of this paper is organized as follows. In Sec. II, we present the calculation formulas of the BBC function for hydrodynamic sources. In Sec. III, we investigate the BBC functions of  $\phi\phi$  for hydrodynamic sources with different initial geometries and energy densities. The oscillations of BBC functions as a function of the particle momentum and the

dependences of BBC functions on the directions of the particle momentum are also discussed in this section. Finally, a summary and conclusions of this paper are given in Sec. IV.

## II. CALCULATIONS OF BBC FUNCTIONS FOR HYDRODYNAMIC SOURCES

The description of ideal hydrodynamics for the system with zero net-baryon density is defined by the local conservations of energy and momentum [9, 10],

$$\partial_\mu T^{\mu\nu}(r) = 0, \quad (10)$$

where  $T^{\mu\nu}(r) = [\epsilon(r) + \mathcal{P}(r)] u^\mu(r) u^\nu(r) - \mathcal{P}(r) g^{\mu\nu}$  is the density tensor of energy-momentum ideal fluid at space-time coordinate  $r$ ,  $\epsilon(r)$  and  $\mathcal{P}(r)$  are the energy density and pressure in the local rest frame of the fluid element at  $r$ , which move at velocity  $\mathbf{v}(r)$ ,  $u^\mu = \gamma(1, \mathbf{v})$  is the four-velocity,  $\gamma = (1 - \mathbf{v}^2)^{-1/2}$ , and  $g^{\mu\nu} = \text{diag}(+, -, -, -)$  is the Minkowski metric tensor. Under the assumption of Bjorken longitudinal boost invariance [8], we need only to solve the transverse equations of motion in the  $z = 0$  plane, and the hydrodynamic solutions at  $z \neq 0$  ( $v^z = z/t$ ) can be obtained by the longitudinal boost invariance hypothesis [11, 12].

From Eq. (10) we have the transverse equations in the  $z = 0$  plane,

$$\begin{aligned} \partial_t \mathcal{E} + \partial_x [(\mathcal{E} + \mathcal{P}) v^x] + \partial_y [(\mathcal{E} + \mathcal{P}) v^y] &= -\mathcal{F}(\mathcal{E}, \mathcal{P}, t), \\ \partial_t \mathcal{M}^x + \partial_x (\mathcal{M}^x v^x + \mathcal{P}) + \partial_y (\mathcal{M}^x v^y) &= -\mathcal{G}(\mathcal{M}^x, t), \\ \partial_t \mathcal{M}^y + \partial_x (\mathcal{M}^y v^x) + \partial_y (\mathcal{M}^y v^y + \mathcal{P}) &= -\mathcal{G}(\mathcal{M}^y, t), \end{aligned} \quad (11)$$

where  $\mathcal{E} = T^{00} = \gamma^2(\epsilon + \mathcal{P}) - \mathcal{P}$ ,  $\mathcal{M}^i = T^{0i} = \gamma^2(\epsilon + \mathcal{P})v^i$ , ( $i = x, y$ ),  $\mathcal{F}(\mathcal{E}, \mathcal{P}, t) = (\mathcal{E} + \mathcal{P})/t$ , and  $\mathcal{G}(\mathcal{M}^i, t) = \mathcal{M}^i/t$ . In equation set (11) there are  $\epsilon$ ,  $\mathcal{P}$ ,  $v^x$ , and  $v^y$  four variables. So an equation of state,  $\mathcal{P}(\epsilon)$ , is needed to enclose the equation set. In the calculations, we use the equation of state of s95p-PCE, which combines the hadron resonance gas at low temperatures and the lattice QCD results at high temperatures [20]. We assume that the system reaches the static local equilibrium at  $\tau_0 = 0.6$  fm/c after the collision, and take the initial energy density distribution in the transverse plane as the Gaussian distribution,

$$\epsilon = \epsilon_0 \exp[-x^2/(2R_x^2) - y^2/(2R_y^2)], \quad (12)$$

where  $\epsilon_0$  and  $R_i$  ( $i = x, y$ ) are the parameters of the initial source energy density and radii. With the equation of state and the initial energy density we can solve equation set (11) using the relativistic HLLC scheme and Sod's operation splitting method [9, 13, 21–26].

For hydrodynamic sources, with the formula derived by Makhlin and Sinyukov [27], the chaotic and squeezed amplitudes can be expressed as [2, 3]

$$G_c(\mathbf{k}_1, \mathbf{k}_2) = \int \frac{d^4\sigma_\mu(r)}{(2\pi)^3} K_{1,2}^\mu e^{i q_{1,2} \cdot r} \left\{ |c'_{\mathbf{k}'_1, \mathbf{k}'_2}|^2 n'_{\mathbf{k}'_1, \mathbf{k}'_2} + |s'_{-\mathbf{k}'_1, -\mathbf{k}'_2}|^2 [n'_{-\mathbf{k}'_1, -\mathbf{k}'_2} + 1] \right\}, \quad (13)$$

$$G_s(\mathbf{k}_1, \mathbf{k}_2) = \int \frac{d^4\sigma_\mu(r)}{(2\pi)^3} K_{1,2}^\mu e^{2i K_{1,2} \cdot r} \left\{ s'^*_{-\mathbf{k}'_1, \mathbf{k}'_2} c'_{\mathbf{k}'_2, -\mathbf{k}'_1} \times n'_{-\mathbf{k}'_1, \mathbf{k}'_2} + c'_{\mathbf{k}'_1, -\mathbf{k}'_2} s'^*_{-\mathbf{k}'_2, \mathbf{k}'_1} [n'_{\mathbf{k}'_1, -\mathbf{k}'_2} + 1] \right\}. \quad (14)$$

Here  $d^4\sigma_\mu(r)$  is the four-dimension element of freeze-out hypersurface,  $q_{1,2}^\mu = k_1^\mu - k_2^\mu$ ,  $K_{1,2}^\mu = (k_1^\mu + k_2^\mu)/2$ , and  $\mathbf{k}'_i$  is the local-frame momentum corresponding to  $\mathbf{k}_i$  ( $i = 1, 2$ ). The other local variables are:

$$c'_{\pm\mathbf{k}'_1, \pm\mathbf{k}'_2} = \cosh[f'_{\pm\mathbf{k}'_1, \pm\mathbf{k}'_2}], \quad (15)$$

$$s'_{\pm\mathbf{k}'_1, \pm\mathbf{k}'_2} = \sinh[f'_{\pm\mathbf{k}'_1, \pm\mathbf{k}'_2}], \quad (16)$$

$$\begin{aligned} f'_{\pm\mathbf{k}'_1, \pm\mathbf{k}'_2} &= \frac{1}{2} \log \left[ (\omega'_{\mathbf{k}'_1} + \omega'_{\mathbf{k}'_2}) / (\Omega'_{\mathbf{k}'_1} + \Omega'_{\mathbf{k}'_2}) \right] \\ &= \frac{1}{2} \log \left[ K_{1,2}^\mu u_\mu(r) / K_{1,2}^{*\nu} u_\nu(r) \right] \\ &\equiv f_{\mathbf{k}_1, \mathbf{k}_2}(r), \end{aligned} \quad (17)$$

$$\begin{aligned} \omega'_{\mathbf{k}'_i}(r) &= \sqrt{\mathbf{k}'_i{}^2(r) + m^2} = k_i^\mu u_\mu(r) \\ &= \gamma_{\mathbf{v}} [\omega_{\mathbf{k}_i} - \mathbf{k}_i \cdot \mathbf{v}(r)], \end{aligned} \quad (18)$$

$$\begin{aligned} \Omega'_{\mathbf{k}'_i}(r) &= \sqrt{\mathbf{k}'_i{}^2(r) + m_*^2} \\ &= \sqrt{[k_i^\mu u_\mu(r)]^2 - m^2 + m_*^2} \\ &= k_i^{*\mu} u_\mu(r), \end{aligned} \quad (19)$$

$$\begin{aligned} n'_{\pm\mathbf{k}'_1, \pm\mathbf{k}'_2} &= \exp \left\{ - \left[ \frac{1}{2} (\Omega'_{\mathbf{k}'_1} + \Omega'_{\mathbf{k}'_2}) - \mu_{1,2}(r) \right] / T(r) \right\} \\ &= \exp \left\{ - [K_{1,2}^{*\mu} u_\mu(r) - \mu_{1,2}(r)] / T(r) \right\} \\ &\equiv n_{\mathbf{k}_1, \mathbf{k}_2}(r), \end{aligned} \quad (20)$$

where,  $K_{1,2}^{*\mu} = (k_1^{*\mu} + k_2^{*\mu})/2$  is the pair four-momenta of the quasiparticles in medium, and  $u^\mu(r) = \gamma_{\mathbf{v}}[1, \mathbf{v}(r)]$ ,  $\mu_{1,2}(r)$ , and  $T(r)$  are the source four-velocity, the pair chemical

potential, and the source temperature at particle freeze-out, respectively. Equation (19) gives the relationship between  $k^{*\mu}u_\mu(r)$  and  $k^\mu u_\mu(r)$ , which is used in calculating  $f_{\mathbf{k}_1, \mathbf{k}_2}(r)$  and  $n_{\mathbf{k}_1, \mathbf{k}_2}(r)$ .

### III. BBC RESULTS FOR HYDRODYNAMIC SOURCES

#### A. Source distributions

For hydrodynamic sources with a Bjorken cylinder, the four-dimension element of the freeze-out hypersurface can be written as

$$d^4\sigma_\mu(r) = f_\mu(\tau, \mathbf{r}_\perp, \eta) d\tau d^2\mathbf{r}_\perp d\eta, \quad (21)$$

where  $\tau$ ,  $\mathbf{r}_\perp$ , and  $\eta$  are the proper time, transverse coordinate, and space-time rapidity of the element. The function  $f_\mu(\tau, \mathbf{r}_\perp, \eta)$  is related to the freeze-out mechanism that is considered, and  $K_{1,2}^\mu f_\mu(\tau, \mathbf{r}_\perp, \eta)$  corresponds to the source distributions of proper time and space in the calculations [see Eqs. (13) and (14)]. In this work we assume that  $\phi$  mesons are frozen out at a fixed temperature  $T_f$  and use the AZHYDRO technique [10, 18, 19] to calculate the freeze-out hypersurface element.

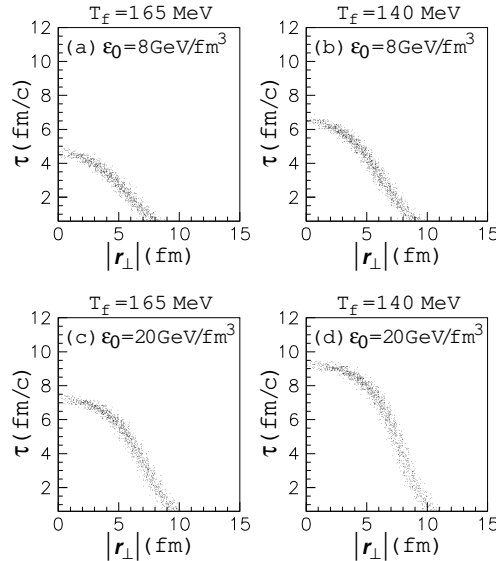


FIG. 1: Distributions of the freeze-out points of  $\phi$  mesons in the  $z = 0$  plane for the initial conditions  $\epsilon_0 = 8$  and  $20 \text{ GeV}/\text{fm}^3$  and  $R_x = R_y = 4 \text{ fm}$ .

We show in Fig. 1 the distributions of the freeze-out points (source points) of  $\phi$  mesons in the  $z = 0$  plane for the initial conditions  $\epsilon_0 = 8$  and  $20 \text{ GeV}/\text{fm}^3$  and  $R_x = R_y = 4 \text{ fm}$ . The distribution profile for the lower  $T_f$  is wider than that for the higher  $T_f$  because of the source expansion. And the distribution profiles increase with increasing initial energy density. In Fig. 2, we show the normalized distributions of the transverse coordinate and time of the  $\phi$  freeze-out points in the  $z = 0$  plane, which are obtained by projecting the two-dimensional distributions in Fig. 1 to the coordinate and time axes, respectively. One can see that the transverse-coordinate distributions are similar to Gaussian distributions. The temporal distributions increase with time nonlinearly and have sharp falls to 0 at long evolving times. The widths of the spatial and temporal distributions increase with increasing initial energy density and decrease with increasing freeze-out temperature.

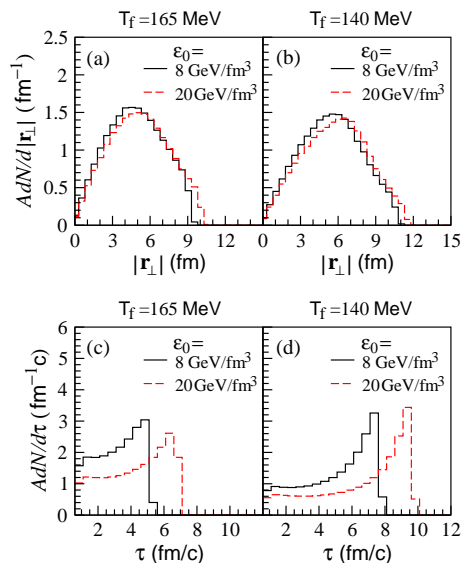


FIG. 2: (Color online) Normalized distributions of transverse coordinate and time of the  $\phi$  freeze-out points in the  $z = 0$  plane for the same initial conditions as in Fig. 1.

## B. BBC functions

In Fig. 3, we plot the BBC functions of  $\phi\phi$  in  $k - m_*$  plane for the hydrodynamic sources with different initial radii and energy densities. In the calculations, we take  $\eta$  in the region  $(-1, 1)$  and the chemical potential of boson-antiboson pairs,  $\mu_{1,2}(r) = 0$ . The freeze-out temperature of  $\phi$  meson is taken to be  $140 \text{ MeV}$  [3–7]. The variation of the BBC functions

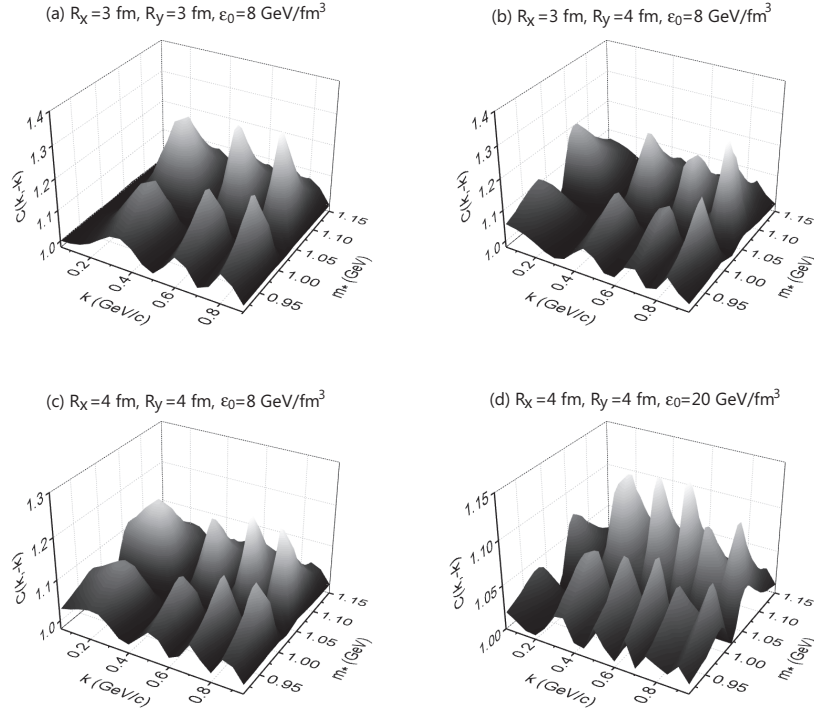


FIG. 3: BBC functions of  $\phi\phi$  for the hydrodynamic sources with different initial conditions and  $T_f = 140$  MeV.

with the modified mass  $m_*$  is similar to that of the BBC functions calculated previously [3–7]. However, the BBC functions for hydrodynamic sources exhibit oscillations as a function of  $k$ , compared to the BBC functions for sources with Gaussian spatial distributions and a temporal distribution of the exponential decay [3–7].

To examine the reason for the oscillations of BBC functions, we calculate the BBC functions for sources with spatial distributions obtained from the hydrodynamic freeze-out points,  $dN/d|\mathbf{r}_\perp|$ , [see Figs. 2(a) and 2(b)], and the parameterized temporal distribution,

$$F(\tau) = (a + b\tau^2) \theta(\tau - \tau_0) \theta(\tau_{\max} - \tau), \quad (22)$$

where  $a$ ,  $b$ , and  $\tau_{\max}$  are three parameters. As shown in Fig. 4, temporal distributions  $F_1$  and  $F_2$  are similar to the distributions in Fig. 2(d). In Fig. 4, the thin solid line is for the temporal distribution of the exponential decay [3–7]. It is much different from the distributions of Eq. (22). We plot in Fig. 5 the BBC functions of  $\phi\phi$  for sources with hydrodynamic spatial distributions [see Fig. 2(b)] and parameterized temporal distributions of Eq. (22) and exponential decay (see Fig. 4). Here, Figs. 5(a) and 5(b) are with temporal

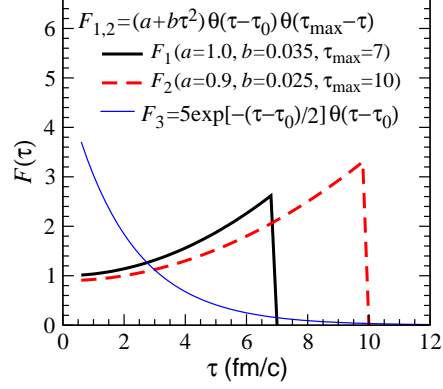


FIG. 4: (Color online) Parameterized temporal distributions  $F_1$  and  $F_2$  in Eq. (22) for the parameter sets  $[a = 1.0 \text{ (fm/c)}^{-1}, b = 0.035 \text{ (fm/c)}^{-3}, \tau_{\text{max}} = 7 \text{ fm/c}]$  and  $[a = 0.9 \text{ (fm/c)}^{-1}, b = 0.025 \text{ (fm/c)}^{-3}, \tau_{\text{max}} = 10 \text{ fm/c}]$ . The thin solid (blue) line  $F_3$  is for the temporal distribution of the exponential decay.

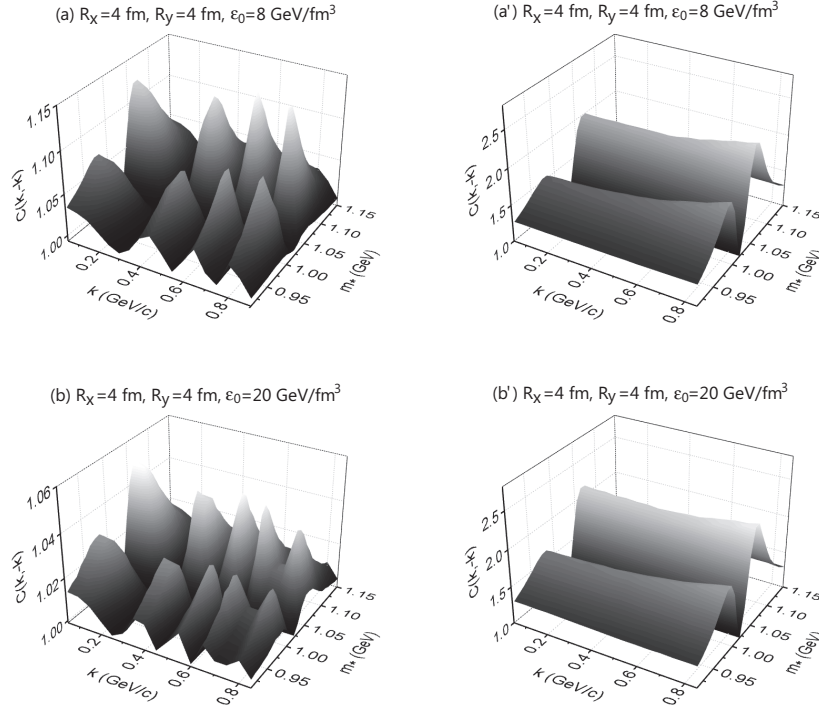


FIG. 5: BBC functions of  $\phi\phi$  for the sources with hydrodynamic spatial distributions [see Fig. 2(b)] and parameterized temporal distributions (see Fig. 4). (a, b) With temporal distributions  $F_1$  and  $F_2$  in Fig. 4; (a', b') with temporal distribution  $F_3$  in Fig. 4.

distributions  $F_1$  and  $F_2$  in Fig. 4, and Figs. 5(a') and 5(b') are with temporal distribution  $F_3$  in Fig. 4. In the calculations, the source temperature is taken to be  $T_f = 140 \text{ MeV}$ ,

and the source velocities used are still the hydrodynamic source velocities at the freeze-out points. One can see that there are oscillations in the BBC functions calculated with temporal distributions  $F_1$  and  $F_2$ , which have sharp falls to 0 at long times. However, the oscillations disappear in the BBC functions calculated with the temporal distribution of exponential decay,  $F_3$ . The peak values of the BBC functions for temporal distributions  $F_1$  and  $F_2$  are smaller than those of the BBC functions for temporal distribution  $F_3$ . The reason, as will be seen, is that the width of temporal distribution  $F_3$  is much smaller than those of  $F_1$  and  $F_2$ .

In the calculations of the BBC functions with parameterized temporal distributions, we have

$$C(\mathbf{k}, -\mathbf{k}) = 1 + \frac{\left| \int_{\eta_1}^{\eta_2} D_\eta(k) I_\eta^s(\mathbf{k}) d\eta \right|^2}{\left[ \int_{\eta_1}^{\eta_2} I_\eta^c(\mathbf{k}) d\eta \right] \left[ \int_{\eta_1}^{\eta_2} I_\eta^c(-\mathbf{k}) d\eta \right]}, \quad (23)$$

where

$$D_\eta(k) = \frac{\int F(\tau) e^{i2\omega_k \tau \cosh \eta} d\tau}{|\eta_2 - \eta_1| \int F(\tau) d\tau}, \quad (24)$$

$$I_\eta^s(\mathbf{k}) = \int \frac{dN}{d^2\mathbf{r}_\perp} [s_{\mathbf{k}, -\mathbf{k}}^*(r) c_{-\mathbf{k}, \mathbf{k}}(r) n_{\mathbf{k}, -\mathbf{k}}(r) + c_{\mathbf{k}, -\mathbf{k}}(r) s_{-\mathbf{k}, \mathbf{k}}^*(r) (n_{\mathbf{k}, -\mathbf{k}}(r) + 1)] d^2\mathbf{r}_\perp, \quad (25)$$

$$I_\eta^c(\mathbf{k}) = \int \frac{dN}{d^2\mathbf{r}_\perp} [|c_{\mathbf{k}, \mathbf{k}}(r)|^2 n_{\mathbf{k}, \mathbf{k}}(r) + |s_{\mathbf{k}, \mathbf{k}}(r)|^2 (n_{\mathbf{k}, \mathbf{k}}(r) + 1)] d^2\mathbf{r}_\perp, \quad (26)$$

$$c_{\mathbf{k}_1, \mathbf{k}_2}(r) = \cosh[f_{\mathbf{k}_1, \mathbf{k}_2}(r)], \quad s_{\mathbf{k}_1, \mathbf{k}_2}(r) = \sinh[f_{\mathbf{k}_1, \mathbf{k}_2}(r)]. \quad (27)$$

For the parameterized temporal distribution in Eq. (22), we have

$$|D_\eta(k)| = \frac{[b^2 d^4 + 4a(a + bd^2) \sin^2(d\sqrt{m^2 + k^2} \cosh \eta)]^{1/2}}{2\sqrt{m^2 + k^2} \cosh \eta (ad + bd^3/3) |\eta_2 - \eta_1|}, \quad (28)$$

where  $d = (\tau_{\max} - \tau_0)$ , and the approximation  $b \ll a(m^2 + k^2)(\cosh \eta)^2 / (c\hbar)^2$  is taken. The oscillations of the BBC functions are from  $D_\eta(k)$ . We plot  $|D_\eta(k)|$  in Fig. 6 for the parameterized temporal distributions in Eq. (22) (thick lines) and the temporal distribution of exponential decay (thin lines), in this case  $|D_\eta(k)| = \{(\eta_2 - \eta_1)^2 [1 + 4(m^2 + k^2) \cosh^2 \eta \Delta t^2]\}^{-1/2}$  and  $\Delta t = 2 \text{ fm}/c$ . We take  $\eta_1 = -1$  and  $\eta_2 = 1$  in the calculations. The magnitudes of  $D_\eta(k)$  behave as oscillations for the parameterized temporal distributions  $F_1$  because of the sharp falls in the distributions at long times (see thick lines in Fig. 4). However, the magnitudes of  $D_\eta(k)$  for the temporal distribution of the exponential decay,  $F_3$  in Fig. 4, are smoothed. The magnitude of  $D_\eta(k)$  for  $F_3$  are larger than those for  $F_1$  because the width of the  $F_3$  distribution is smaller than that of  $F_1$ . For all the temporal distributions, the magnitude of

$D_\eta(k)$  decreases with increasing  $\eta$ . And, the BBC functions are determined by the product of  $D_\eta(k)$  and  $I_\eta^s(k)$ .

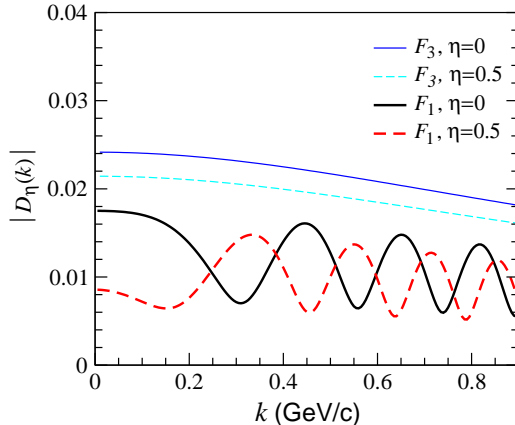


FIG. 6: (Color online) Magnitudes of  $D_\eta(k)$  for temporal distributions  $F_1$  and  $F_3$  in Fig. 4.

### C. Dependence of the BBC function on the direction of the particle momentum

For anisotropic sources, the BBC functions depend not only on the magnitude of the particle momentum, but also on its direction [7]. This is because the source velocities in different directions lead to the variation of  $k^\mu u_\mu$  with the momentum direction. To examine the dependence of the BBC functions on the direction of the particle momentum, we use

$$\cos \alpha = k_z/|\mathbf{k}|, \quad \cos \beta = k_x/|\mathbf{k}_T|, \quad (|\mathbf{k}_T| = \sqrt{k_x^2 + k_y^2}), \quad (29)$$

to describe the direction of the particle momentum.  $\alpha$  and  $\beta$  are the polar angle and azimuthal angle of the particle. In Fig. 7, we plot the BBC functions of  $\phi\phi$  in the  $\cos \beta$ - $k$  plane for hydrodynamic sources with different initial radii and energy densities. Here,  $m_*$  is taken as 1.05 GeV, corresponding to approximately the peaks of the BBC functions (see Fig. 3). For  $R_x < R_y$ , the source expanding velocity in the  $x$  direction is higher than that in the  $y$  direction. The BBC functions for sources with  $R_x < R_y$  are larger at  $\cos \beta = 0$  than those at  $\cos \beta = 1$ , because the average values of  $e^{-k^\mu u_\mu/T_f}$  are smaller at  $\cos \beta = 0$  than that at  $\cos \beta = 1$  in this case [7]. For the source with  $R_x = R_y$ , the BBC functions are independent of  $\cos \beta$ .

In Fig. 8, we show the dependence of the average BBC functions,  $\langle C(k, -k) \rangle_k$ , of  $\phi\phi$  on the cosine of the particle azimuthal angle for hydrodynamic sources with different initial radii

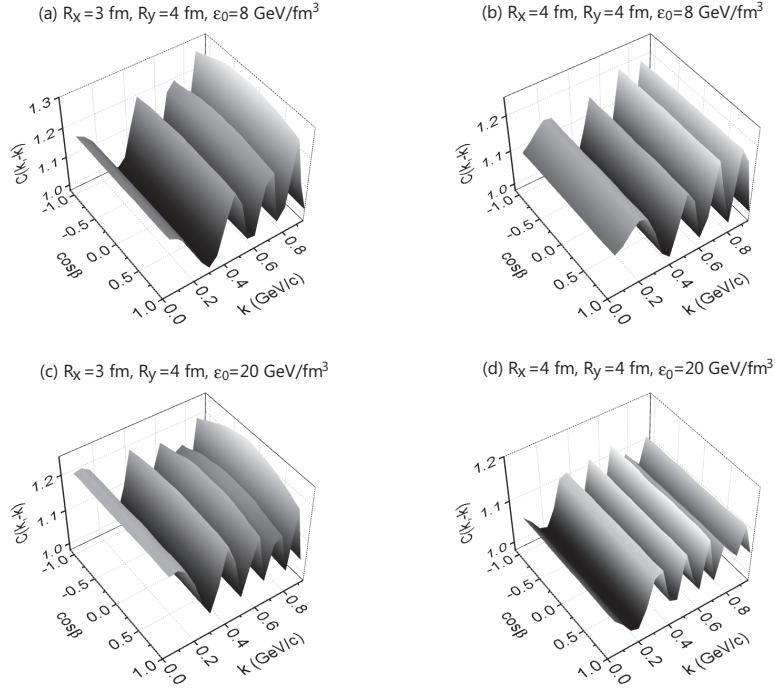


FIG. 7: BBC functions of  $\phi\phi$  in the  $\cos\beta$ - $k$  plane for hydrodynamic sources with different initial radii and energy densities. Here,  $m_*$  is taken as 1.05 GeV.

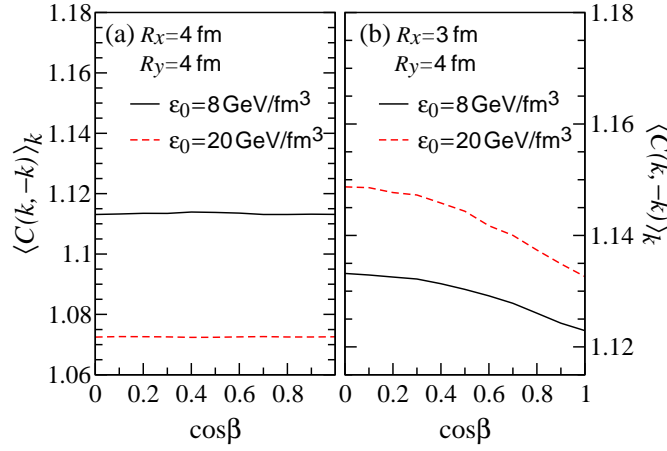


FIG. 8: (Color online) Dependence of the average BBC functions,  $\langle C(k, -k) \rangle_k$ , of  $\phi\phi$  on the cosine of the particle azimuthal angle for hydrodynamic sources with different initial radii and energy densities. Here,  $m_*$  is taken as 1.05 GeV and the momentum region averaged is 0–1 GeV/c.

and energy densities. Here,  $m_*$  is taken as 1.05 GeV and the momentum region averaged is 0–1 GeV/c. The BBC functions are independent of the azimuthal angle for transverse isotropic sources. However, the BBC functions for transverse anisotropic sources increase

with increasing azimuthal angle of the particles ( $0 < \beta < \pi/2$ ). For transverse isotropic sources, the average BBC function for the higher initial energy density is smaller than that for the lower initial energy density. The reasons are that the source with a higher initial energy density has a larger expansion velocity and a wider temporal distribution of freeze-out points. For transverse anisotropic sources, we observe that the average BBC function for the higher initial energy density is larger than that for the lower initial energy density. This is mainly because the many oscillations of the BBC function for the source with the higher initial energy density lead to an increase in the average value in the momentum region [see Figs. 7(a) and 7(c)].

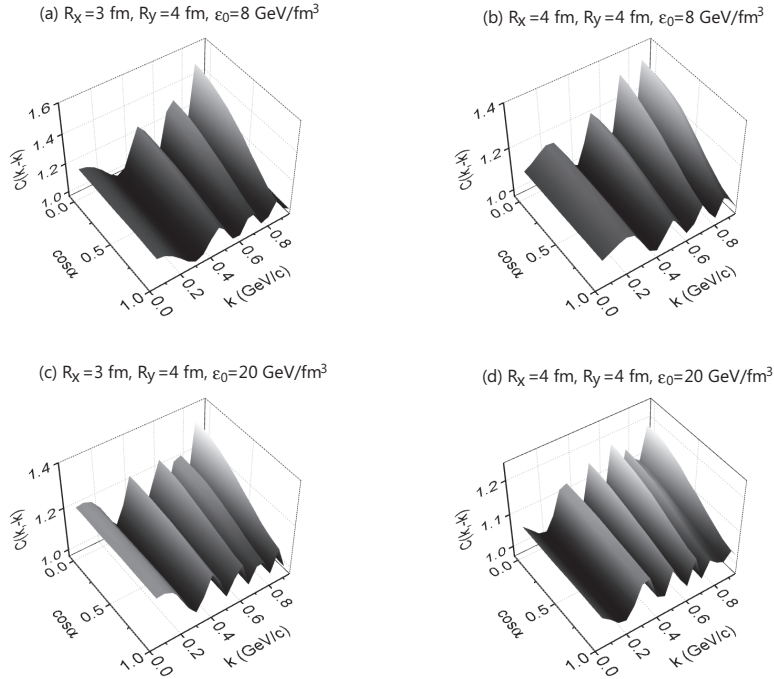


FIG. 9: BBC functions of  $\phi\phi$  in the  $\cos\alpha$ - $k$  plane for hydrodynamic sources with different initial radii and energy densities. Here,  $m_*$  is taken as 1.05 GeV.

We plot in Fig. 9 the BBC functions of  $\phi\phi$  in the  $\cos\alpha$ - $k$  plane for hydrodynamic sources with different initial radii and energy densities, and for  $m_* = 1.05$  GeV. The ridge values of the BBC functions for a fixed  $k$  decrease with increasing  $\cos\alpha$ . The reasons for this are that the average source longitudinal velocity is higher than the average source transverse velocity for hydrodynamic sources with Bjorken longitudinal boost invariance [8], and the higher longitudinal velocity leads to smaller average values of  $e^{-k^\mu u_\mu/T_f}$  at  $\cos\alpha = 0$  than at

$\cos \alpha = 1$  [7].

Because  $\cos \alpha$  is related to particle pseudorapidity by

$$\tilde{y} = \tanh^{-1}(\cos \alpha), \quad (30)$$

the polar angle dependence of the BBC functions can lead to pseudorapidity dependence of the BBC functions. In Fig. 10, we show the dependence of the average BBC functions,  $\langle C(k, -k) \rangle_k$ , of  $\phi\phi$  on the pseudorapidity of the particle for hydrodynamic sources with different initial radii and energy densities. Here,  $m_*$  is taken as 1.05 GeV and the momentum region averaged is 0–1 GeV/c. The BBC functions decrease with increasing  $|\tilde{y}|$  as expected. Because the average transverse velocities for sources with a higher initial energy density are higher than those for sources with a lower initial energy density, the BBC functions for sources with a higher initial energy density decrease more slowly with increasing  $|\tilde{y}|$ .

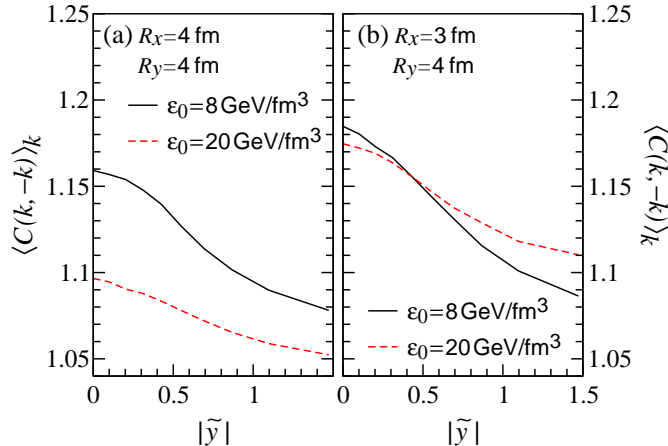


FIG. 10: (Color online) Dependence of the average BBC functions  $\langle C(k, -k) \rangle_k$  of  $\phi\phi$  on the pseudorapidity of the particle for hydrodynamic sources with different initial radii and energy densities. Here,  $m_*$  is taken as 1.05 GeV and the momentum region averaged is 0–1 GeV/c.

#### IV. SUMMARY AND DISCUSSION

In the hot and dense hadronic sources formed in high-energy heavy-ion collisions, particle interactions in medium might lead to a squeezed BBC of boson-antiboson pairs. The investigations of the BBC in previous works are for sources with space-time-separated source distributions [3–7]. The smoothed temporal distribution of the exponential decay scales the

BBC functions and leads to monotonic BBC functions with respect to the particle momentum [3–7].

Relativistic hydrodynamics is successful in describing the source space-time evolution in high-energy heavy-ion collisions. In this paper, we investigate the BBC functions of  $\phi\phi$  for sources evolving hydrodynamically in  $(2 + 1)$  dimensions and with longitudinal boost invariance. For hydrodynamic sources, the BBC functions oscillate as a function of the particle momentum. The reason for the oscillations is that the temporal distributions of sources evolving hydrodynamically have sharp falls to 0 at large evolving times, compared to the temporal distribution of the exponential decay. We also investigate the dependences of the BBC functions on the directions of the particle momentum. For transverse anisotropic sources, the anisotropic source velocity leads to the dependence of the BBC functions on the particle azimuthal angle. The BBC functions are minimum when the azimuthal angles of the particles reach 0. Because the average source longitudinal velocity is higher than the average source transverse velocity, the BBC functions increase with decreasing absolute value of the particle pseudorapidity. The oscillations and the dependences on the particle azimuthal angle and pseudorapidity are the significant signatures for detecting the BBC in high-energy heavy-ion collisions.

For  $\mathbf{k}_1 = \mathbf{k}$ ,  $\mathbf{k}_2 = -\mathbf{k}_1 = -\mathbf{k}$ ,  $e^{2iK_{1,2}\cdot r} = e^{2i\omega_{\mathbf{k}}t}$ , the BBC function  $C(\mathbf{k}, -\mathbf{k})$  for the hydrodynamic source is related to the temporal Fourier transformation of the space-time distribution of source freeze-out points [see Eqs. (4), (13), and (14)]. So, the BBC function is very sensitive to the temporal distribution of the source, and an appropriate source space-time distribution is important for estimating the BBC effect in high-energy-heavy ion collisions. In Refs. [2–7], a sudden freeze-out assumption at time  $\tau_f$  is adopted, and then a parameterized distribution of  $\tau_f$  (exponential decay) is used in the calculations to suppress the BBC functions. In Ref. [28], the author argues the appropriateness of the sudden freeze-out assumption of time and discusses the exponential suppression of the BBC function based on three parameterized temporal distributions. In this work, we extract the space-time distributions of the source from the  $(2 + 1)$ -dimensional hydrodynamics. The temporal and spatial distributions of the source are related in the calculations. Although it is a significant advance compared to the parameterized space-independent distributions of time used in [2–7, 28], further investigations based on more realistic models in which the model parameters are determined by the experimental data on the observables, such as

single particle spectra, elliptic flow, HBT radii, are needed for the expectations of the BBC effect in high-energy heavy-ion collisions.

### Acknowledgments

This research was supported by the National Natural Science Foundation of China under Grant No. 11275037.

- 
- [1] M. Asakawa and T. Csörgő, *Heavy Ion Phys.* **4** (1996) 233; hep-ph/9612331.
  - [2] M. Asakawa, T. Csörgő and M. Gyulassy, *Phys. Rev. Lett.* **83** (1999) 4013.
  - [3] S. S. Padula, G. Krein, T. Csörgő, Y. Hama, P. K. Panda, *Phys. Rev. C* **73** (2006) 044906.
  - [4] D. M. Dudek, S. S. Padula, *Phys. Rev. C* **82** (2010) 034905.
  - [5] S. S. Padula, O. Socolowski, Jr., *Phys. Rev. C* **82** (2010) 034908.
  - [6] Y. Zhang, J. Yang, W. N. Zhang, *Chin. Phys. C* **39** (2014) 034103; arXiv:1406.6446.
  - [7] Y. Zhang, J. Yang, W. N. Zhang, presented at the 2014 Autumn Conference of China Physical Society, Sep. 12-14, 2014, Harbin, China; arXiv:1506.01486.
  - [8] J. D. Bjorken, *Phys. Rev. D* **27** (1983) 140.
  - [9] D. H. Rischke, arXiv:nucl-th/9809044.
  - [10] P. F. Kolb, U. Heinz, arXiv:nucl-th/0305084.
  - [11] G. Baym, B. L. Friman, J. P. Blaizot, M. Soyeur, W. Czyż, *Nucl. Phys. A* **407** (1983) 397.
  - [12] M. Gyulassy, D. H. Rischke, B. Zhang, *Nucl. Phys. A* **613** (1997) 397.
  - [13] D. H. Rischke, S. Bernard, J. A. Maruhn, *Nucl. Phys. A* **595** (1995) 346; D. H. Rischke, M. Gyulassy, *Nucl. Phys. A* **608** (1996) 479.
  - [14] T. Csörgő, B. Lörstad, *Phys. Rev. C* **54** (1996) 1390.
  - [15] M. Csanád, T. Csörgő, B. Lörstad, A. Ster, *J. Phys. G* **30** (2004) S1079.
  - [16] M. Csanád, T. Csörgő, A. Ster, B. Lörstad, N. N. Ajitanand, J. M. Alexander, P. Chung, W. G. Holzmann, M. Issah, R. A. Lacey, *Eur. Phys. J. A* **38** (2008) 363.
  - [17] A. Ster, M. Csanád, T. Csörgő, B. Lörstad, B. Tomášik, *Eur. Phys. J. A* **47** (2011) 58.
  - [18] P. F. Kolb, J. Sollfrank, and U. Heinz, *Phys. Rev. C* **62** (2000) 054909.
  - [19] P. F. Kolb and R. Rapp, *Phys. Rev. C* **67** (2003) 044903.

- [20] C. Shen, U. Heinz, P. Huovinen, H. C. Song, Phys. Rev. C **82** (2010) 054904.
- [21] M. J. Efaaf, W. N. Zhang, M. Khaliliasr et al., High Energy Phys. Nucl. Phys. **29** (2005) 467.
- [22] A. Harten, P. D. Lax. B. van Leer, SIAM Rev., **25** (1983) 35; B. Einfeldt, SIAM J. Numer. Anal., **25** (1988) 294. V. Schneider, U. Katscher, D. H. Rischke et al. J. Comput. Phys. **105** (1993) 92.
- [23] G. A. Sod, J. Fluid Mech. **83** (1977) 785.
- [24] W. N. Zhang, M. J. Efaaf, C. Y. Wong, M. Khaliliasr, Chin. Phys. Lett. **10** (2004) 1918; M. J. Efaaf, W. N. Zhang, M. Khaliliasr et al., High Energy Phys. Nucl. Phys. **29** (2005) 46.
- [25] W. N. Zhang, M. J. Efaaf, C. Y. Wong, Phys. Rev. C **70** (2004) 024903
- [26] L. L. Yu, W. N. Zhang, C. Y. Wong, Phys. Rev. C **78** (2008) 014908; H. J. Yin, J. Yang, W. N. Zhang, L. L. Yu, Phys. Rev. C **86** (2012) 024914.
- [27] A. Makhlin and Yu. M. Sinyukov, Sov. J. Nucl. Phys. **46** (1987) 354; Yu. M. Sinyukov, Nucl. Phys. **A566** (1994) 589c.
- [28] J. Knoll, Phys. Rev. C **83** (2011) 044914.